Contrasting fission potential-energy structure of actinides and mercury isotopes

Takatoshi Ichikawa,[1] Akira Iwamoto,[2] Peter Möller,[3] and Arnold J. Sierk[3]

[1]*Yukawa Institute for Theoretical Physics, Kyoto University, Kyoto 606-8502, Japan*
[2]*Advanced Science Research Center, Japan Atomic Energy Agency, Tokai-mura, Naka-gun, Ibaraki 319-1195, Japan*
[3]*Theoretical Division, Los Alamos National Laboratory, Los Alamos, New Mexico 87545, USA*

Background: Fission-fragment mass distributions are asymmetric in the fission of typical actinide nuclei for nucleon number A in the range $228 \lesssim A \lesssim 258$ and proton number Z in the range $90 \lesssim Z \lesssim 100$. For somewhat lighter systems it has been observed that fission mass distributions are usually symmetric. However, a recent experiment showed that fission of ^{180}Hg following electron capture on ^{180}Tl is asymmetric.

Purpose: We calculate potential-energy surfaces for a typical actinide nucleus and for 12 even isotopes in the range ^{178}Hg–^{200}Hg, to investigate the similarities and differences of actinide compared to mercury potential surfaces and to what extent fission-fragment properties, in particular shell structure, relate to the structure of the static potential-energy surfaces.

Methods: Potential-energy surfaces are calculated in the macroscopic-microscopic approach as functions of five shape coordinates for more than five million shapes. The structure of the surfaces is investigated by the use of an immersion technique.

Results: We determine properties of minima, saddle points, valleys, and ridges between valleys in the five-dimensional shape-coordinate space. Along the mercury isotope chain the barrier heights and the ridge heights and their persistence with elongation vary significantly and show no obvious connection to possible fragment shell structure, in contrast to the actinide region, where there is a deep asymmetric valley extending from the saddle point to scission.

Conclusions: The mechanism of asymmetric fission must be very different in the lighter proton-rich mercury isotopes compared to the actinide region and is apparently unrelated to fragment shell structure. Isotopes lighter than ^{192}Hg have the saddle point shielded from a deep symmetric valley by a significant ridge. The ridge vanishes for the heavier Hg isotopes, for which we would expect a qualitatively different asymmetry of the fragments.

I. INTRODUCTION

The evolution of a nucleus from a single ground-state shape into two separated fragments in nuclear fission has, since its discovery [1], been described in terms of potential-energy surfaces that are functions of suitable shape coordinates [2,3]. Originally the potential energy was modeled in terms of a macroscopic liquid-drop model [2–5]. Subsequently it became clear that the liquid-drop model cannot explain many features of fission, such as the fission-fragment mass yields, fission-barrier structure, and actinide fission half-lives [5–12], because microscopic shell effects significantly perturb the energy surface given by the liquid-drop model. Although the energy release in fission, that is the potential-energy change between the ground state of a single system and well-separated fragments, is more than 200 MeV, microscopic effects in the narrow range of 0 to 10 MeV can affect half-lives by more than ten orders of magnitude and change fission-fragment mass yields from symmetric to significantly asymmetric.

Experimental observations are that fission-fragment mass distributions are asymmetric in low-energy fission of typical actinide nuclei for nucleon number A in the range $228 \lesssim A \lesssim 258$ and proton number Z in the range $90 \lesssim Z \lesssim 100$. In those nuclei, it has been established that the heavy-mass peak in the yield distribution is close to $A = 140$, independently of fissioning system; see, for example [13,14]. This was thought to originate from the strong spherical shell effects present in fragments near the doubly-magic nucleus $^{132}_{50}$Sn$_{82}$,

although we now know that an analysis of high-dimensional potential-energy surfaces [11,12], coupled with a dynamical description, is required to robustly establish this connection [15]. In particular, we now know that "fragment-shell" arguments or saddle-point properties cannot by themselves reliably predict the degree of asymmetry; rather, the character of the entire potential-energy surface between the ground-state and separated fragments must be considered [15,16].

A large-scale experiment studying fission of nuclei in the region $205 \leqslant A \leqslant 234$ showed that a transition to symmetric fission occurred just below the actinide region and that fission remained symmetric at least down to proton number $Z = 85$ and nucleon number $A = 205$. The dividing line between asymmetric and symmetric fission was found to approximately follow constant nucleon number, $A = 226$ [17]. The position of this transition line was predicted to within about two neutrons in a simple static calculation in 1972 [18]. For slightly lighter systems [19,20] near $Z = 82$ and $A = 200$, a hint of asymmetric fission was observed for energies up to about 10 MeV above the saddle-point energy. Itkis *et al*. referred to this as "asymmetry of symmetric fission" [19], so it is unclear whether or not they viewed their results as a clear indication of the onset of a new region of asymmetric fission. Despite this intriguing result, it has often been assumed that fission mass distributions for systems below the actinide region would be symmetric because, based on the proton and neutron numbers of possible compound systems, division into fragments with Z and N sufficiently close to ^{132}Sn (or to much lighter doubly

magic nuclides) so as to exhibit strong shell effects appeared not possible for almost all compound systems below $A \approx 200$. Surprisingly, a recent experiment showed [16] that fission of ^{180}Hg following electron capture by ^{180}Tl is asymmetric.

It was earlier argued that the asymmetric fission of ^{180}Hg was a new type of asymmetric fission with its origins in the local structure of the fission potential-energy surface near the fission saddle point [16]. Moreover, it was argued that these observations showed that the consideration of "fragment shells" does not offer a general method of predicting or explaining asymmetry in fission.

To illustrate the contrasting origins of asymmetric fission in the Hg and actinide regions, we calculate and analyze the structure of five-dimensional fission potential-energy surfaces for even Hg isotopes in the range $178 \leqslant A \leqslant 200$ and compare them to a typical actinide potential-energy surface, namely that of ^{236}U.

II. MODEL

The potential energy is calculated in the finite-range liquid-drop model (FRLDM) [12,21], with the 2002 parameter set for the macroscopic model [22]. We use two shape parametrizations. For more elongated shapes somewhat beyond the ground state, we use the three-quadratic-surface (3QS) parametrization [23,24] to describe nuclear shapes in a five-dimensional deformation space. The shape degrees of freedom are a quadrupole-moment parameter q_2, a neck-related parameter η, heavier- and lighter-fragment deformation parameters ϵ_H and ϵ_L, and a mass-asymmetry parameter α_g. The parameter η is related to the curvature of the middle body. The parameter q_2 is the dimensionless quadrupole moment in units of $3ZR_0^2/4\pi(e^2 b)$, where Z is the proton number and R_0 is the nuclear radius. The parameter ϵ is the Nilsson perturbed-spheroid parameter. The mass-asymmetry parameter is $\alpha_g = (M_H - M_L)/(M_H + M_L)$, where M_H and M_L are the masses of the heavier and lighter nascent fragments, respectively. For finite neck radii these masses are defined as discussed in Ref. [11]. The microscopic single-particle potential is calculated by folding a Yukawa function over the shape of a "sharp-surface generating volume" [25].

We calculate adiabatic potential-energy surfaces in this five-dimensional deformation space for the 12 even isotopes in the range $^{178-200}$Hg and for ^{236}U and analyze their structures using the immersion method [12]. The potential energies are determined at $41 \times 15 \times 15 \times 15 \times 35$ grid points for $q_2 \times \eta \times \epsilon_H \times \epsilon_L \times \alpha_g$. For q_2 and η we use similar, and for fragment deformations and asymmetry α_g exactly, the same points as in Ref. [12]. We take into account the shape-dependent Wigner and A^0 terms in our calculations [12].

Near the ground states where $q_2 \leqslant 0.5$, we also perform complementary constrained-multipole (β_2) calculations, which better describe compact shapes for small deformations [21]. We identify the minima and potential valleys under the condition that their depths are deeper than 0.05 and 0.2 MeV, respectively. In our static studies we can make realistic determinations of major features in the potential-energy surfaces, such as minima, saddles, valleys, and ridges between valleys, because in our model we (1) calculate the

energy in millions of grid points for the five most essential shape degrees of freedom and (2) use an immersion method to extract structure features [12]. In contrast, in self-consistent methods in which *constraints* are imposed, the inferred saddle points and ridges may be overestimated by amounts that can be quite large. Moreover, the magnitude of this overestimation is impossible to determine; see Ref. [12] for a detailed discussion.

III. CALCULATED STRUCTURE OF POTENTIAL-ENERGY SURFACES

In the early days of theoretical fission studies based on the macroscopic-microscopic method, most or all investigations calculated the fission potential-energy surface in terms of only two independent shape variables, for example variables related to elongation and neck radius [7,26] or elongation and fragment mass asymmetries [10]. Complete results from such calculations could be faithfully displayed in terms of two-dimensional contour diagrams. In contrast, it is impossible to show all essential features of five-dimensional potential surfaces by reducing them to two-dimensional contour plots. To identify major features of the five-dimensional (5D) spaces, we start by locating all minima, saddles, ridges, and valleys by the use of the immersion technique; for details see Ref. [12]. We then show features identified to be of special interest in one-dimensional plots versus quadrupole moment. For example, we show the energies along specific one-dimensional paths, such as valleys and ridges, embedded in the full 5D space and relevant minima and saddles. To more clearly visualize the substantial differences of asymmetric fission in the neutron-deficient Hg region and actinide region, we will also plot 2D surfaces embedded in the full 5D deformation space.

Figures 1 and 2 show calculated "optimal" one-dimensional potential-energy curves or "fission barriers," embedded in the five-dimensional space, as functions of q_2 (solid black line) for ^{180}Hg and ^{198}Hg, respectively. In this study, all potential
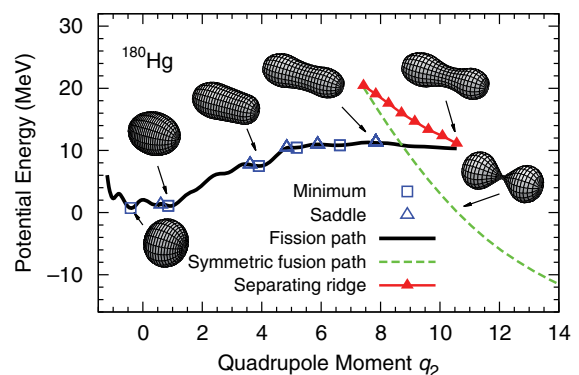

FIG. 1. (Color online) Potential energy along two valleys (paths) and one ridge, and at minima and saddle points for ^{180}Hg versus q_2 from oblate shapes to very deformed configurations. The solid (black) line denotes the optimum fission path leading to a mass-asymmetric split. The gray (green) dashed line denotes a symmetric valley in the potential-energy surface, corresponding to a compact fusion valley with zero-radius neck shapes along the entire valley. The solid (red) line with superimposed triangles is the ridge separating those two valleys.
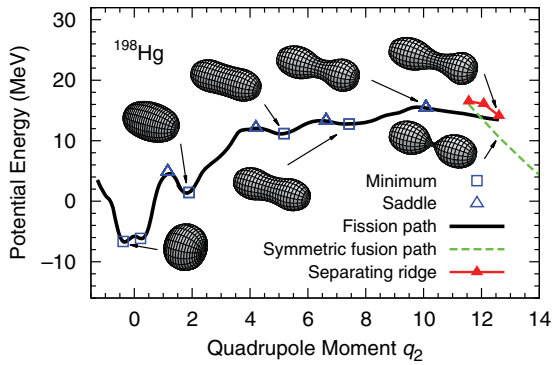
FIG. 2. (Color online) Potential energy along two valleys (paths) and one ridge, and at minima and saddle points for ^{198}Hg versus q_2 from oblate shapes to very deformed configurations. The dashed line is a symmetric valley corresponding to a fusion valley with deformed shapes connected by a conicoidal neck region. The symbols are the same as in Fig. 1.

energies are given relative to the spherical macroscopic energy. Minima and saddle points are indicated by open squares and triangles, respectively. Shapes of the nuclear macroscopic densities at several saddle points and minima are also displayed.

In both systems the ground-state shapes are slightly oblate. However, the density evolutions from the ground state to the fission saddle points differ substantially. For ^{180}Hg, mass asymmetry has developed already near the local energy minimum at $q_2 = 4.0$, although no distinct fragments have yet emerged; cf. Fig. 1. Subsequently the neck develops, while the degree of mass asymmetry is retained. At the fission saddle point $E_{sad} = 11.35$ MeV, and its shape corresponds to $q_2 = 7.84$, $\epsilon_H = 0.275$, $\epsilon_L = 0.30$, and $\alpha_g = 0.14$ or equivalently $A_H/A_L = 102.6/77.4$.

On the other hand, the shape for ^{198}Hg remains symmetric up to the local energy minimum at $q_2 = 7.5$, although the neck is well developed there. Beyond this local minimum, the mass asymmetry of the fissioning nuclei develops in tandem with neck formation. At the fission saddle point $E_{sad} = 15.47$ MeV, $q_2 = 10.08$, $\epsilon_H = 0.35$, $\epsilon_L = 0.10$, and $\alpha_g = 0.12$, or equivalently $A_H/A_L = 110.9/87.1$.

In the outer saddle region additional valleys appear in the two potential-energy surfaces. For each of the two systems we show only one of these valleys, namely the one corresponding to symmetric shapes as dashed (green) lines. To leave the figures uncluttered we do not show an asymmetric valley which is also present. Often these valleys are referred to as *fusion* valleys because along the entire curve the neck radius is zero. In a more general treatment allowing for a family of shapes of separated nuclei, the fragments, or equivalently, the two colliding heavy ions, would be separated along this curve until they have approached sufficiently close that they touch. Separated fragments are inaccessible in the 3QS parametrization in its current implementation. Instead these configurations are represented as two spheroidal nascent fragments connected by a conicoidal neck [23,24]. This limitation does not affect our study here, since we only follow the shape evolution until just before zero neck radius (in a

more general treatment, separation) occurs. What we wish to establish here is the structure of the potential-energy surface from outside the saddle point to just before separation. Is it possible to determine if it favors evolution towards the symmetric valley or the asymmetric valley? And when is the final fragment asymmetry established? Clearly it will be frozen in prior to reaching the bottom of any of the valleys, since zero-neck-radius shapes occur already above the valley floors. For ^{180}Hg, the shape configuration in the symmetric fusion valley is two spherical shapes with ^{90}Zr $+ ^{90}$Zr, which exists because in the macroscopic model, symmetric separated fragments are energetically favored over asymmetric fragments, and the $N = 50$ shell favors spherical fragments. The nascent fragment shapes in the symmetric fusion valley for ^{198}Hg are fairly deformed with $\epsilon = 0.275$, because the fragment neutron numbers are $N = 59$, corresponding to the onset of deformation in separated nuclei.

An important feature for ^{180}Hg is that the optimal potential-energy curve from the ground state across the saddle and somewhat beyond and the symmetric fusion valley are well separated by the potential ridge, which initially is 8 MeV above the saddle region. On the other hand, the height of the corresponding ridge for ^{198}Hg is much lower (initially only 2 MeV high) and only persists for a narrow range in q_2, suggesting that a change from the asymmetric shapes along the initial fission path to different final fragment mass asymmetries is less hindered in ^{198}Hg than in ^{180}Hg.

The separating ridge for ^{180}Hg vanishes at $q_2 = 10.31$, $\epsilon_H = 0.30$, $\epsilon_L = 0.15$, and $\alpha_g = 0.20$ corresponding to $A_H/A_L = 108.0/72.0$. For ^{198}Hg, the ridge vanishes at $q_2 = 13.47$, $\epsilon_H = 0.40$, $\epsilon_L = 0.0$, and $\alpha_g = 0.18$, corresponding to $A_H/A_L = 115.82/81.82$. At the point where the separating ridge vanishes, no "obvious" valley connects this location to a scission configuration. Instead we are on a rather flat potential-energy surface which in the full 5D space gently slopes in many directions. An analogy is being just below the top of a gently sloping hill. Therefore we cannot determine a plausible optimum fission path by a static analysis alone. However, when the neck is quite well developed where the ridge disappears, it was suggested that the mass asymmetry here might to a significant extent be preserved in the separated fission fragments [16].

IV. SADDLE FEATURES AND FISSION-FRAGMENT MASS ASYMMETRY IN MERCURY ISOTOPES

The fragment mass asymmetry in fission is affected by the saddles, ridges, and valleys in the fission potential-energy surface that appear beyond the fission isomeric minimum. We have identified these features using the immersion method. The results are summarized in Figs. 3 and 4. We pay particular attention to the point where the ridge between the optimal fission path and the fusion valleys disappears, which for ^{180}Hg occurs at $q_2 = 10.31$. For the nuclei we study, it is not possible to identify a clear mass-asymmetric fission path, because the "fission valley" that takes us across the saddle point disappears at elongations slightly beyond the saddle. That is, there is no continuous asymmetric valley from the region of the saddle
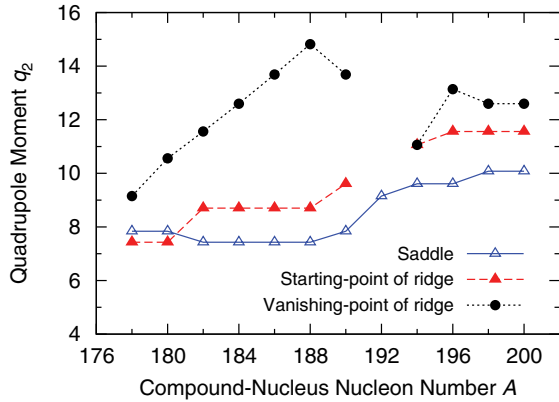
FIG. 3. (Color online) Saddle and ridge locations for a range of Hg isotopes. An extended ridge is only present for isotopes in the interval $180 \leqslant A \leqslant 190$. For $A = 192$ we could not clearly establish the ridge features so data are omitted for this isotope.

point to scission, very much in contrast to the situation in the actinide region.

The mass-symmetric fusion path shown in Fig. 1 corresponds to compact, nearly spherical fragment shapes. This type of fusion valley is only present in Hg nuclei from $A = 178$ to $A = 190$. The ridges separating the compact mass-symmetric fusion path from the asymmetric fission path become very low, almost nonexistent, at $A = 190$, and this compact symmetric fusion valley vanishes at $A = 192$. Instead, for somewhat heavier isotopes a mass-symmetric fusion path with large nascent-fragment deformations appears. To summarize, some general trends in the structure of the potential-energy surfaces along the Hg isotope chain are:

(a) With increasing A the barrier height increases, partly due to a lowering of the ground state as $N = 126$ is approached, and also to a decrease of fissility.

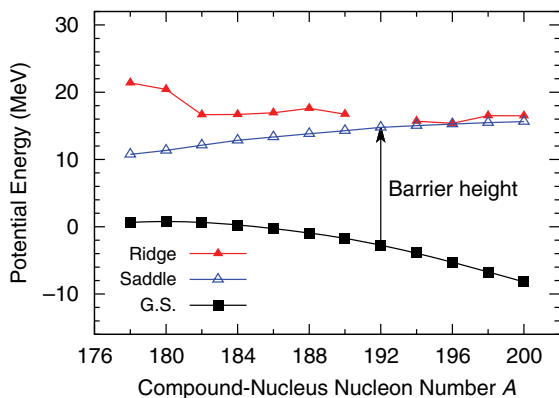(b) The saddle shapes are more elongated (larger q_2) for the heavier Hg isotopes.

FIG. 4. (Color online) Ground-state energy, saddle energy, and maximum ridge height, all with respect to the spherical macroscopic energy. The difference between the saddle energy and the ground-state energy is the barrier height, as indicated with an arrow for ^{192}Hg. It is only for isotopes in the interval $178 \leqslant A \leqslant 190$ that a ridge rises above the saddle.
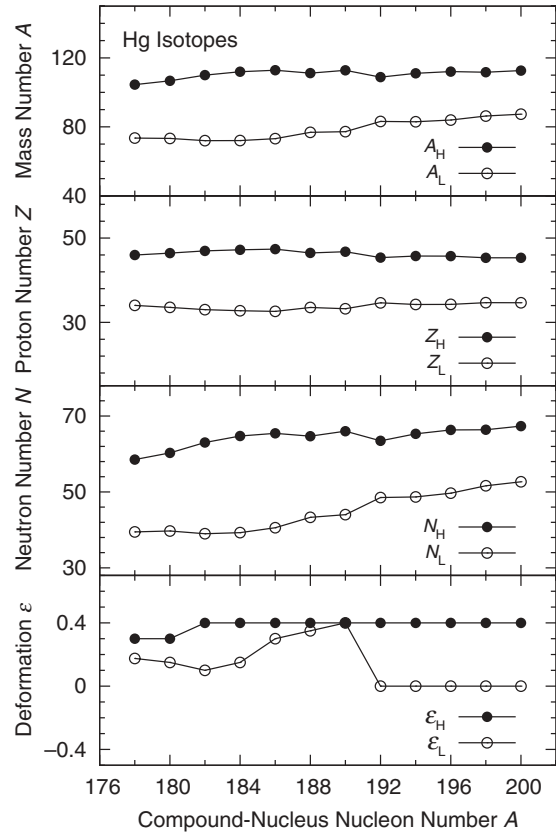

FIG. 5. (Top) Mass number, (Second) proton number, (Third) neutron number, and (Bottom) deformation of the heavy and light nascent fission fragments at the vanishing point of the separating ridge determined from wave-function densities in the two fragments by methods described in Ref. [27].

(c) For low A the ridges are prominent; for higher A, they almost disappear.

In the specific case of electron-capture-delayed fission of ^{180}Hg, the shape asymmetry where the ridge vanishes could be related to the observed fission-fragment mass asymmetry [16]. In Fig. 5 we show the asymmetry at this vanishing point for the entire range of isotopes. We calculate the asymmetry from the wave-function densities (top three panels); cf. Ref. [27] for details. In the bottom panel we show the nascent-fragment shape-deformation parameters at this point. These features stand out:

(i) The proton number of the light (heavy)-mass fragment is close to $Z = 34(46)$ in all the Hg isotopes (see the second panel). However, no strong shell effect is present in the ground states of these fragments. The ground-state shapes for all the $Z = 34(46)$ fragments are well deformed with uniformly positive microscopic corrections [21].

(ii) The neutron number of the light-mass fragment is close to $N = 50$ for $A > 190$, and the deformation of those light fragments is spherical (cf. the third panel).

(iii) At the vanishing point of the ridge the degree of fragment mass asymmetry becomes smaller with increasing mass number. But for the heavier isotopes the ridge is

very short and low in energy so the asymmetry at the vanishing point might not be closely related to the final fragment mass asymmetry.

V. TWO TYPES OF ASYMMETRIC FISSION

Asymmetric fission in the actinide region has since its discovery been "explained" in terms of strong "shells" in the heavy fragment related to its proximity to doubly magic ^{132}Sn. But it should be observed that in fission of actinides, the heavy fragment is not exactly ^{132}Sn and just small changes in Z and N from the doubly magic nucleus drastically decrease the extra binding due to the proximity to a doubly closed shell. For example, the most probable mass split of ^{240}Pu is $M_{\mathrm{H}}/M_{\mathrm{L}} = 140/100$. This corresponds to the heavy fragment $^{140}_{55}$Cs$_{85}$ with a ground-state microscopic correction of -2.96 MeV [21], which is not even close to the ^{132}Sn ground-state microscopic correction of -11.55 MeV. But, when the nascent fragments start to emerge, they have not absorbed some nucleons in the neck regions. Thus, the partially formed heavy fragment in the case of ^{240}Pu is closer in size and shape to ^{132}Sn than it is to $^{140}_{55}$Cs$_{85}$, which could significantly affect the microscopic correction. For example, just removing one proton and one neutron from $^{140}_{55}$Cs$_{85}$ leads to $^{138}_{54}$Xe$_{84}$, with a ground-state microscopic correction of -5.35 MeV [21].

Clearly, one should only invoke such hand-waving arguments related to fragment properties as a starting point for understanding the mass-asymmetric fission-fragment division in the actinide region. A more complete understanding should involve the potential energy from the ground-state shape to separated fragments in terms of a sufficiently large number of shape degrees of freedom [11]. It has indeed been shown that a deep asymmetric valley separated from a symmetric fission valley for most actinides extends from the saddle region to scission configurations [11,12]. As an example, we show in Fig. 6 calculated energies along symmetric and asymmetric optimal fission paths and the separating ridge
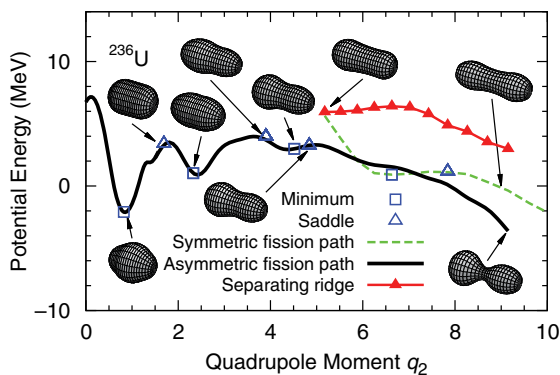

FIG. 6. (Color online) Potential energy along two valleys (paths) and one ridge, and at minima and saddle points for ^{236}U from a spherical shape to very deformed configurations. Here the symmetric valley is well separated from the asymmetric valley by a ridge that is about 5 MeV high along the entire deformation range between the saddle and the asymmetric scission configuration.
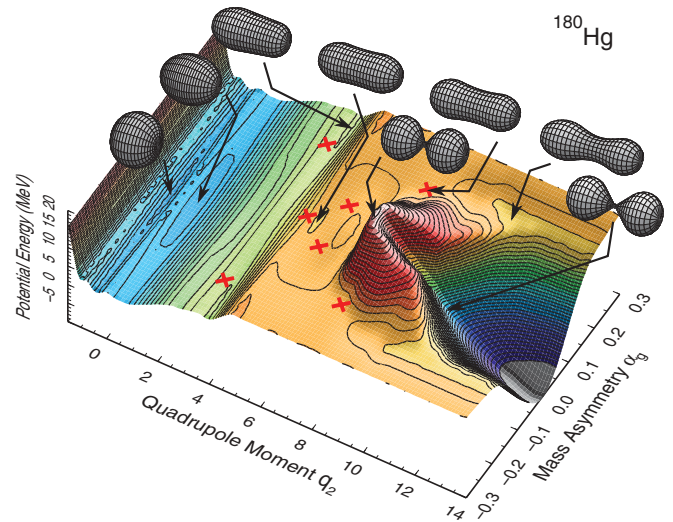

FIG. 7. (Color online) Two-dimensional potential-energy surface for ^{180}Hg which shows some essential features of the full 5D potential-energy surface. Two crossed (red) lines show the locations of some saddle points. Note in particular that the valley across the asymmetric saddle disappears slightly beyond $q_2 = 10$.

for ^{236}U. Here an asymmetric valley extends from the outer saddle region to scission. It is shielded from the symmetric valley by an about five-MeV-high ridge along its entire path. This contrasts very much with the situation in the Hg region.

To illustrate more clearly the differences between Hg and actinides in the fission potential-energy surfaces, in particular the presence and absence of fragment shell effects in the potential-energy surfaces of the compound system, we plot in Fig. 7 a by necessity somewhat schematic two-dimensional representation of the most important features of the full 5D
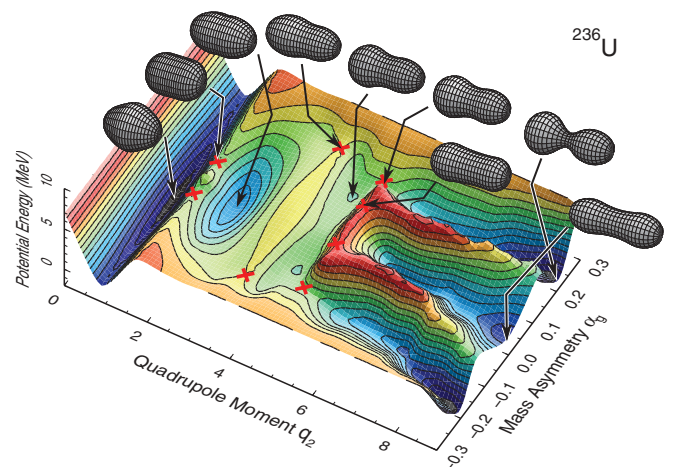

FIG. 8. (Color online) Two-dimensional potential-energy surface for ^{236}U which shows some essential features of the full 5D potential-energy surface. Two crossed (red) lines show the locations of some saddle points. Note in particular that the valley across the asymmetric saddle continues to the largest q_2 shown. It also continues beyond to a point where the nucleus separates into two fragments. This is very much in contrast to the potential-energy surface for ^{180}Hg.
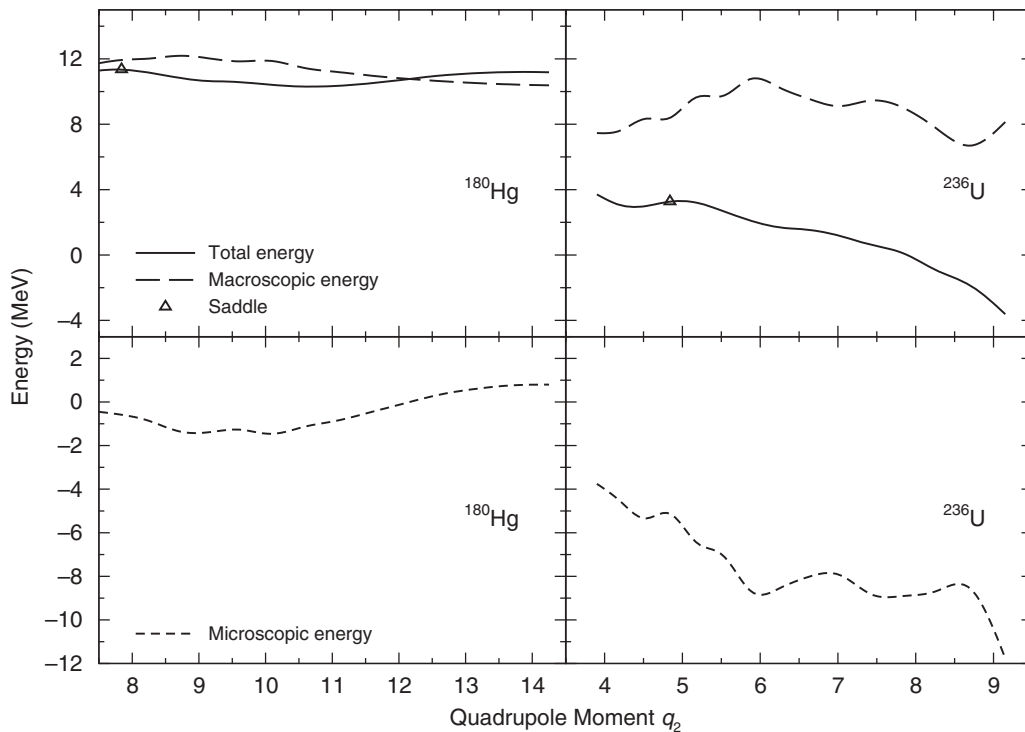
FIG. 9. Total and macroscopic energies along the asymmetric fission paths for ^{180}Hg and ^{236}U are shown in the top two frames. The microscopic energies along these paths are shown in the lower two frames. There are very significant differences between the microscopic energies of the two nuclei.

potential-energy surface for ^{180}Hg. In the left part of Fig. 9 we show the total energy, macroscopic energy, and microscopic energy along a section of the asymmetric fission path of ^{180}Hg. In Fig. 8 and the right part of Fig. 9 we show the corresponding quantities for ^{236}U.

These figures illustrate visually the different origins of asymmetric fission in the Hg and actinide regions. For ^{236}U the asymmetric valley extends from the outer saddle point to scissionlike shapes. It is a plausible assumption that the mean asymmetry in thermal neutron-induced fission is close to the asymmetry of the shapes at the bottom of the asymmetric valley. This correlation was indeed verified in the investigation of Ref. [11] in which the calculated asymmetry of the asymmetric valley bottom agreed with observed fission-fragment mass asymmetries for 25 even-even actinide nuclei with a mean deviation of only 3.0 nucleons. The large negative microscopic energy $E_{sh} = -12$ MeV at scission where $q_2 = 9$, cf. Fig. 9, remains almost constant for more compact shapes; it is still very substantial, $E_{sh} = -6$ MeV, at the saddle-point deformation $q_2 = 5$.

In contrast, for ^{180}Hg there is no valley extending from the saddle region towards scission. Rather, for elongations only moderately beyond the saddle, the ridge separating the saddle region and the symmetric fusion valley disappears. From static considerations alone, it is not obvious what trajectory towards separated fragments the nucleus will follow. Thus, as stated in Ref. [16], the asymmetric fission in ^{180}Hg is a new type of asymmetric fission with its origins in the local fission potential-energy-surface structure in the saddle region, whereas in the actinide region a deep, persistent asymmetric valley extends

over the entire range from saddle-point shapes to separated fragments. Figure 9 shows that there is no significant fragment-related microscopic effect in the saddle region or beyond for ^{180}Hg; this microscopic energy is very low, fluctuating between ± 2 MeV along the trajectory shown.

VI. SUMMARY DISCUSSION

The recent observation of mass asymmetry in electron-capture delayed fission of ^{180}Hg [16] has stimulated renewed interest in fission since some simple fragment-shell type arguments had anticipated that the most probable division would be into two symmetric ^{90}Zr fragments, because these exhibit two instances of the spherical $N = 50$ magic number and two instances of the spherical $Z = 40$ subshell. It was proposed that a new type of asymmetric fission had been observed, with its origins in the *local* structure in the outer saddle-point region. Currently, the experimental data in this neutron-deficient region in terms of energy range and number of nuclides are extremely sparse, in particular in comparison with the data available for heavier nuclei [14,28]. We have calculated potential-energy surfaces of 12 even Hg isotopes in this neutron-deficient region to establish the systematics of significant structures. The most important finding is that it is only for nuclei in the range $180 \lesssim A \lesssim 190$ that the saddle region is somewhat shielded from the symmetric fusion valley by a moderately high ridge that also has some moderate extension in the elongation direction. In the ^{180}Hg experiment the compound-nucleus excitation was limited to about 1 MeV

above the saddle point. This constraint and the ridge structure allowed some qualitative conclusions about the expected fragment asymmetries in this experiment [16].

In the actinide region numerous models have been proposed to describe the observed fission mass asymmetries, for example, Refs. [15,28–33]. Often encouraging results are presented. We have shown here and elsewhere [11,12] that in calculated, realistic 5D potential-energy surfaces, very strongly expressed, deep asymmetric valleys are present. These valleys usually appear also in more approximate calculations, so that when the respective model parameters are adjusted to experimental yields the model results agree to varying degrees of accuracy with the experimental data. However none of these models has been applied to ^{180}Hg, with the exception of the Brownian shape-motion model [15,34], in which no parameter is adjusted. Although the statistics of the ^{180}Hg experiment are limited, the Brownian shape-motion model may be less accurate in this case than in the actinide region since for ^{180}Hg the result was $M_H/M_L = 104.4/75.6$ whereas the experimental result was given as $M_H/M_L = 100/80$. More striking is that the calculated full width at half maximum (FWHM) [34] is about twice the experimental result of nine mass units [16]. In the actinide region the calculated widths agreed very well with the experimental data [15] with no obvious deviations except in the tails of the yield distributions at very large asymmetries. A possible explanation of these results is that in the actinide region the confining influence of the steep walls of the asymmetric valley defines the width of the yield distributions, and this feature is realistically described in the calculations. In the Hg region, where there are no confining fission valley walls, the yield distribution is determined on the downslope of a steep, smooth mountain side; cf. Fig. 7. Here the fine details of the dynamical part of the model may be more important than in the actinide region. The models in the other Refs. [28–33] have not yet been tested in this mass region.

Clearly, it will be a challenge to fission theories to reproduce experimental data both in the Hg region and across the entire actinide region without arbitrary model parametrizations which differ from region to region. Since we have now shown the different issues presented to theory by fission in the Hg and actinide regions, we strongly encourage efforts to obtain a more extensive set of fission data in the region $180 \leqslant A \leqslant 200$ be undertaken, both in terms of excitation-energy range and number of nuclides. Such experiments would present new and highly useful challenges to fission theories.

[1] O. Hahn and F. Strassmann, Naturwiss. **27**, 11 (1939).

[2] L. Meitner and O. R. Frisch, Nature (London) **143**, 239 (1939).

[3] N. Bohr and J. A. Wheeler, Phys. Rev. **56**, 426 (1939).

[4] S. Frankel and N. Metropolis, Phys. Rev. **72**, 914 (1947).

[5] D. L. Hill and J. A. Wheeler, Phys. Rev. **89**, 1102 (1953).

[6] W. J. Swiatecki, Phys. Rev. **100**, 937 (1955).

[7] V. M. Strutinsky, Nucl. Phys. A **95**, 420 (1967).

[8] V. M. Strutinsky, Ark. Fys. **36**, 629 (1967).

[9] V. M. Strutinsky, Nucl. Phys. A **122**, 1 (1968).

[10] P. Möller and S. G. Nilsson, Phys. Lett. B **31**, 283 (1970).

[11] P. Möller, D. G. Madland, A. J. Sierk, and A. Iwamoto, Nature (London) **409**, 785 (2001).

[12] P. Möller, A. J. Sierk, T. Ichikawa, A. Iwamoto, R. Bengtsson, H. Uhrenholt, and S. Åberg, Phys. Rev. C **79**, 064304 (2009).

[13] L. Wilets, *Theories of Nuclear Fission* (Clarendon Press, Oxford, 1964).

[14] R. Vandenbosch and J. R. Huizenga, *Nuclear Fission* (Academic Press, New York, 1973).

[15] J. Randrup and P. Möller, Phys. Rev. Lett. **106**, 132503 (2011).

[16] A. N. Andreyev *et al.*, Phys. Rev. Lett. **105**, 252502 (2010).

[17] K.-H. Schmidt, J. Benlliure, and A. R. Junghans, Nucl. Phys. A **693**, 169 (2001).

[18] P. Möller, Nucl. Phys. A **192**, 529 (1972).

[19] M. G. Itkis, N. A. Kondrat'ev, S. I. Mul'gin, V. N. Okolovich, A. Ya. Rusanov, and G. N. Smirenkin, Yad. Fiz. **52**, 944 (1990).

[20] M. G. Itkis, N. A. Kondrat'ev, S. I. Mul'gin, V. N. Okolovich, A. Ya. Rusanov, and G. N. Smirenkin, Yad. Fiz. **53**, 1225 (1991).

[21] P. Möller, J. R. Nix, W. D. Myers, and W. J. Swiatecki, At. Data Nucl. Data Tables **59**, 185 (1995).

[22] P. Möller, A. J. Sierk, and A. Iwamoto, Phys. Rev. Lett. **92**, 072501 (2004).

[23] J. R. Nix, University of California Radiation Laboratory Report No. UCRL-17958, 1968 (unpublished).

[24] J. R. Nix, Nucl. Phys. A **130**, 241 (1969).

[25] M. Bolsterli, E. O. Fiset, J. R. Nix, and J. L. Norton, Phys. Rev. C **5**, 1050 (1972).

[26] S. G. Nilsson, C. F. Tsang, A. Sobiczewski, Z. Szymański, S. Wycech, C. Gustafson, I.-L. Lamm, P. Möller, and B. Nilsson, Nucl. Phys. A **131**, 1 (1969).

[27] T. Ichikawa, A. Iwamoto, and P. Möller, Phys. Rev. C **79**, 014305 (2009).

[28] K.-H. Schmidt, S. Steinhäuser, C. Böckstiegel, A. Grewe, A. Heinz, A. R. Junghans, J. Benlliure, H.-G. Clerc, M. de Jong, J. Müller, M. Pfützner, and B. Voss, Nucl. Phys. A **665**, 221 (2000).

[29] P. Fong, Phys. Rev. **102**, 434 (1956).

[30] B. D. Wilkins, E. P. Steinberg, and R. R. Chasman, Phys. Rev. C **14**, 1832 (1976).

[31] U. Brosa, S. Grossman, and A. Müller, Phys. Rep. **197**, 167 (1990).

[32] J. Benlliure, A. Grewe, M. de Jong, K.-H. Schmidt, and S. Zhdanov, Nucl. Phys. A **628**, 458 (1998).

[33] H. Goutte, J. F. Berger, P. Casoli, and D. Gogny, Phys. Rev. C **71**, 024316 (2005).

[34] P. Möller, J. Randrup, and A. J. Sierk, Phys. Rev. C **85**, 024306 (2012).